



Enhancement of superconductivity by frustrating the charge order

Zi-Xiang Li , Marvin L. Cohen, and Dung-Hai Lee*

*Department of Physics, University of California, Berkeley, California 94720, USA
and Materials Sciences Division, Lawrence Berkeley National Laboratory, Berkeley, California 94720, USA*

 (Received 20 January 2019; revised manuscript received 7 February 2019; published 4 December 2019)

We study strong electron-phonon interacting systems where the geometry of the crystalline lattice frustrates the formation of charge order. Our results show that under such condition, high- T_c superconductivity can occur in a wide range of electron-phonon coupling strengths. This result is obtained by studying the Holstein model on triangular lattice using sign-problem-free quantum Monte Carlo method.

DOI: [10.1103/PhysRevB.100.245105](https://doi.org/10.1103/PhysRevB.100.245105)

I. INTRODUCTION

Strong electron-phonon (e-ph) interaction is often thought as good for high-temperature superconductivity (SC). However, there are numerous examples where strong e-ph interaction triggers charge order (CO), which in turn suppresses superconductivity. This problem has been appreciated in the literature for a long time [1–13]. Based on such realization, attempts to estimate the upper bound of T_c have been made. This issue has received renewed interest recently where sign-problem-free quantum Monte Carlo (QMC) simulation was used to study the interplay between CO and SC on *unfrustrated* lattice [14].

In this work we ask “what if the CO is geometrically frustrated,” and under that condition “will high- T_c superconductivity result from strong e-ph interaction.” Examples of materials showing geometrically frustrated CO [15] include Fe_3O_4 [16], molecular conductor $\theta\text{-ET}_2\text{X}$ [17], and triangular lattice systems such as LuFe_2O_4 [18], Na_xCoO_2 [19], AlV_2O_4 [20], and LiV_2O_4 [20,21], etc. Among them, $\theta\text{-ET}_2\text{X}$ [22] and Na_xCoO_2 [19] are superconductors.

Our results show that once the CO is frustrated, Cooper pairing is left to benefit from the strong e-ph interaction. Therefore, when the bottleneck for the onset of superconductivity is the Cooper pair formation, high T_c will result from frustrating the CO. However, T_c will not increase with the e-ph interaction forever. Because as the e-ph interaction gets too strong, the Cooper pair becomes so tightly bound that its hopping amplitude becomes suppressed. Under that condition the bottleneck for the onset of superconductivity is the establishment of phase coherence. When that happens, T_c will eventually decrease due to the poor Cooper pair mobility.

It is important to note, however, that our results apply only to systems where Cooper pairing is mediated by phonon. Hence, unconventional superconductors such as cuprates and iron-based superconductors are beyond the scope of this paper.

The theoretical model we study is the Holstein model on the triangular lattice (where geometric frustration of CO exists). When the same model is studied on the square lattice

(where the CO is not frustrated), Ref. [14] shows that as the e-ph interaction gets strong, the $\mathbf{Q} = (\pi, \pi)$ charge density wave (CDW) susceptibility surpasses that of SC. Moreover, when this happens, the Migdal-Eliashberg (ME) theory fails. Physically, this is due to the formation of bipolarons. The CO involves bipolarons occupying one of the sublattices so that each doubly occupied site is surrounded by the empty ones because in such an arrangement electrons on the doubly occupied sites can virtually hop to the neighboring sites to gain the kinetic energy. This is similar to the superexchange mechanism of repulsive systems.

In order to determine the effect of frustration, we compare the results of Holstein’s model on both square and triangular lattices. Following Ref. [14] we quantify the strength of the e-ph interaction by the dimensionless parameter $\lambda = \alpha^2 \rho(E_F)/K$, where $\rho(E_F)$ is the density of states at the Fermi energy and α is the e-ph interaction parameter [see Eq. (1)] and K is the local phonon spring constant. The main results are summarized in the following for the parameter range $0.2 \leq \lambda \leq 0.8$ and $\hbar\omega/E_F = 0.1$ and 0.3 at different electron densities and temperatures. Here, $\omega = \sqrt{K/M}$ is the phonon frequency (M is the mass of the local oscillator.)

(1) For the half-filled square lattice at $T = 0$ we find $\mathbf{Q} = (\pi, \pi)$ CDW order for the entire range of λ we studied. (2) For a half-filled triangular lattice at $T = 0$, on the other hand, we find SC order in the entire range of λ . In contrast, the CDW order [with $\mathbf{Q} = (\pm 4\pi/3, 0)$] only exists for $0.4 \lesssim \lambda \leq 0.8$ when $\hbar\omega/E_F = 0.1$, and for $0.6 \lesssim \lambda \leq 0.8$ when $\hbar\omega/E_F = 0.3$. (3) For the half-filled triangular lattice with $\lambda = 0.4$ (where SC is strongest) we determine the Kosterlitz phase transition temperature to be $T_c \approx t/10$. (4) In the SC-CDW coexistence phase at, e.g., $\hbar\omega/E_F = 0.1$, charge fluctuations are significantly stronger on one sublattice of the tripartite triangular lattice (see discussion below). Moreover, the SC order parameter is the strongest on this sublattice. Through these sites SC can survive at strong e-ph coupling even after the CDW order has set in. (5) At half-filling, a single-particle gap exists in the non-SC phase for both square and triangular lattices.

The results summarized above make the case that the frustration of CDW allows SC to benefit from stronger e-ph coupling without being preempted by the charge order.

*Corresponding author: dunghai@berkeley.edu

Before discussing the details, we present a physical picture which enables one to understand the above results. When λ becomes sufficiently strong, bipolarons form. In the charge-ordered phase, the bipolarons are localized. For the square lattice, which is bipartite, the bipolarons localize on one of the sublattices so that virtual hopping can lower the kinetic energy. For the triangular lattice, however, such an arrangement is impossible. This is the same as the frustration encountered in the antiferromagnetic (AF) Ising model on a triangular lattice. This obstruction toward charge order benefits SC. To understand the coexistence phase, we note that the ground state of the AF Ising model is macroscopically degenerate [$\exp(cN)$ ($c \sim O(1)$)] spin patterns have the same energy] [23–25]. Moreover, it has been shown that out of these degenerate spin patterns, a class of $\sqrt{3} \times \sqrt{3}$ spin configurations [characterized by $\mathbf{Q} = (\pm\frac{4\pi}{3}, 0)$ wave vectors] are selected at zero temperature due to an “order by disorder” mechanism [26,27]. For spin- $\frac{1}{2}$ quantum model, with nearest-neighbor XY exchange, quantum fluctuations stabilize $\sqrt{3} \times \sqrt{3}$ spin long-range order [28–34]. In the present problem we expect the analogous CDW pattern, with $S^z = +1 \rightarrow$ double occupancy and $S^z = -1 \rightarrow$ unoccupancy [see Fig. 1(a)], to be stabilized by either thermal or the quantum fluctuations (introduced by the hopping of electrons). This expectation is supported by the simulation result: The strongest CDW susceptibility is associated with wave vector $(\pm\frac{4\pi}{3}, 0)$ as shown in Fig. 1(b). The same order by disorder mechanism predicts charge fluctuation to be significantly stronger on one of the three $\sqrt{3} \times \sqrt{3}$ sublattices. Each site in this sublattice is surrounded by a hexagon of sites where the charge density alternates between $\langle n_i \rangle > 1$ and $\langle n_i \rangle < 1$. These sites are analogous to the “flippable sites” in the entropy-stabilized $\sqrt{3} \times \sqrt{3}$ pattern of the AF Ising model (spins on the flippable sites are surrounded by alternating spin ups and spin downs, hence, they feel no internal field). Through these large charge fluctuation sites, SC can survive even after the CDW order has set in.

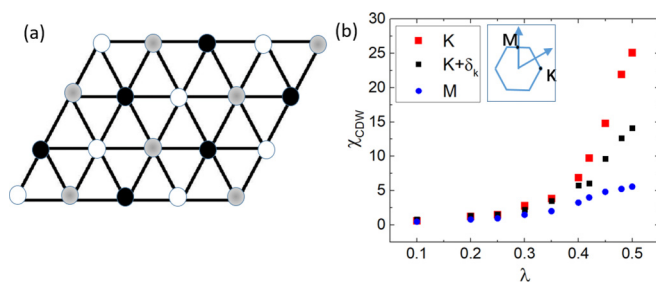


FIG. 1. (a) A schematic figure of the $\sqrt{3} \times \sqrt{3}$ CDW ordered state in the strong e-ph coupling limit on triangular lattice. The ordering wave vectors are $(\pm 4\pi/3, 0)$. The black circles represent the sites with $\langle n_i \rangle > 1$ and the white circles represent sites with $\langle n_i \rangle < 1$. The gray circles stand for sites where large charge fluctuations and $\langle n_i \rangle \approx 1$. (b) The CDW susceptibility at different momenta for the triangular lattice, where $\hbar\omega/E_F$ is set to 0.3 and the temperature is set to $k_B T = t/16$. Here, $\mathbf{K} = (4\pi/3, 0)$, and $\mathbf{M} = (0, 2\pi/\sqrt{3})$ and $\mathbf{K} + \delta_k$ is a momentum closest to \mathbf{K} on a lattice with linear dimension $L = 12$.

II. MODEL

In the following discussions we consider the Holstein model defined on both square and triangular lattices $H = H_e + H_p + H_{ep}$ where

$$H_e = - \sum_{\langle ij \rangle, \sigma} t_{ij} (\psi_{i,\sigma}^\dagger \psi_{j,\sigma} + \text{H.c.}) - \mu \sum_i \hat{n}_{i,\sigma},$$

$$H_p = \sum_i \left(\frac{\hat{p}_i^2}{2M} + \frac{K}{2} \hat{X}_i^2 \right); H_{ep} = \alpha \sum_i \hat{n}_i \hat{X}_i. \quad (1)$$

Here, $\psi_{i,\sigma}$ annihilates an electron with spin polarization σ on lattice site i , μ is the chemical potential, and \hat{n}_i is the electron number operator associated with site i . For the triangular lattice we set the hopping integrals t_{ij} to 1 between nearest neighbors. For the square lattice we set the nearest-neighbor hopping integral to 1 and second-neighbor hopping integral to -0.2 to avoid a nested Fermi surface at half-filling. In the rest of the paper we use t to denote the nearest-neighbor hopping matrix element for both triangular and square lattices. H_p describes a dispersionless Einstein phonon with frequency $\omega = \sqrt{K/M}$, where \hat{X}_i is the phonon displacement operator and \hat{P}_i is its conjugate momentum. H_{ep} describes the e-ph coupling with α being the coupling constant. As mentioned earlier, the e-ph coupling strength is characterized using the dimensionless parameter $\lambda = \alpha^2 \rho(E_F)/K$.

Due to the presence of time-reversal symmetry and particle-number conservation in the electronic part of the action for arbitrary phonon configurations the partition function of Eq. (1) is free of the fermion minus sign problem where it is subjected to determinant QMC simulation [35–41]. In the literature, many QMC simulations have been applied to the Holstein model on nonfrustrated lattices [14,42–52]. Here, the introduction of lattice frustration is a new aspect. We perform zero and nonzero temperature QMC simulations by employing both the single and global update schemes [53]. The details of the QMC simulations can be found in Appendix A.

III. ZERO-TEMPERATURE AND HALF-FILLING

A. Phase diagram

We employ projector QMC [35,54–56] to study the ground state of Eq. (1) for $\hbar\omega/E_F = 0.1, 0.3$ and $0.2 \leq \lambda \leq 0.8$ at zero temperature. Through a finite-size scaling analysis for systems with linear dimension $L = 6, 9, 12, 15$ (the details can be found in Appendix D), we obtain the zero-temperature phase diagrams in the specified range of λ as shown in Figs. 2(a) and 2(b). For the triangular lattice [Fig. 2(a)], SC long-range order exists in the entire range of λ we studied. Moreover, this is true for both $\hbar\omega/E_F = 0.1$ and 0.3. However, for $\hbar\omega/E_F = 0.1$, CDW sets in to coexist with SC for $0.4 \lesssim \lambda \leq 0.8$. For $\hbar\omega/E_F = 0.3$, CDW order is weakened but it still sets in to coexist with SC for $0.6 \lesssim \lambda \leq 0.8$. The CDW ordering wave vectors are $\mathbf{Q} = (\pm 4\pi/3, 0)$ and a schematic figure of it is given in Fig. 1(a). In contrast, for the square lattice there is no SC order (at least within the lattice sizes we studied). Instead, we find CDW order in the entire λ range we studied [see Fig. 2(b)]. The ordering wave vector is

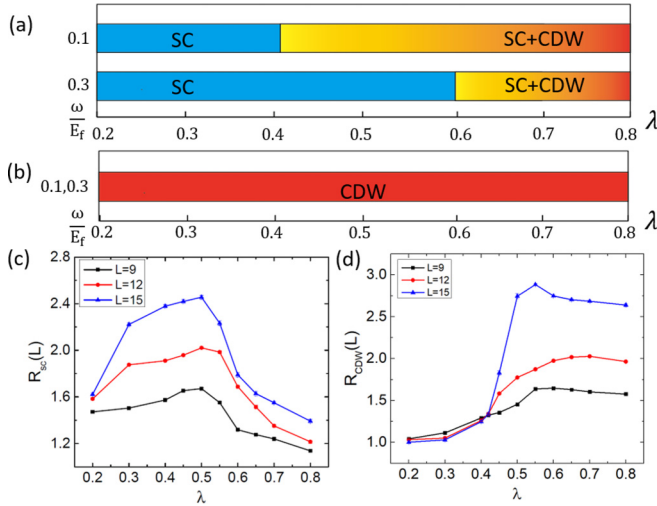


FIG. 2. (a) The zero-temperature phase diagram of the Holstein model in the e -ph coupling range $0.2 \leq \lambda \leq 0.8$ and $\hbar\omega/E_F = 0.1, 0.3$ for the triangular lattice. (b) The same plot for the square lattice. (c) The RG invariant ratio, $R_{SC}(L)$, for the SC order at $\hbar\omega/E_F = 0.1$ on half-filled triangular lattice. The result indicates SC long-range order. (d) The RG invariant ratio, $R_{CDW}(L)$, for the CDW order at $\hbar\omega/E_F = 0.1$ on half-filled triangular lattice. The result is indicative of CDW disorder-order phase transition at $\lambda \approx 0.42$.

$\mathbf{Q} = (\pi, \pi)$. Note that our phase diagram excludes $\lambda < 0.2$. This is because for small λ , weak SC or CDW orders can be suppressed by the nonzero energy gap caused by the finite lattice size, and hence prevent us from drawing conclusions in the thermodynamic limit. However, we do expect the presence of SC order in the thermodynamic limit due to the standard argument that SC is the generic instability for Fermi surface possessing time-reversal symmetry. Because the band structure does not possess Fermi-surface nesting there is no CDW instability. In Figs. 2(c) and 2(d) we present the “RG-invariant ratio” $R = S(\mathbf{Q})/S(\mathbf{Q} + \delta\mathbf{q})$ as a function of system size L for the SC and CDW orders. Here, $S(\mathbf{Q})$ is the Fourier transform of the SC/CDW correlation functions, and $\mathbf{Q} = (0, 0)$ for SC, and $\mathbf{Q} = (\pi, \pi)$ or $(\pm 3\pi/4, 0)$ for the CDW on the square and triangular lattices. $\delta\mathbf{q}$ is a small wave vector introduced to enable a comparison between the correlation function at the expected ordering wave vector and a wave vector nearby, explicitly $\delta\mathbf{q} = (0, \frac{2\pi}{L})$ on square lattice and $\delta\mathbf{q} = (0, \frac{4\pi}{\sqrt{3}L})$ on triangular lattice. Long-range order implies the divergence of R as $L \rightarrow \infty$, while short-range order means $R \rightarrow 1$. The results clearly support the phase diagram presented in Fig. 2(a). Comparing the results for the square and triangular lattices, we conclude that frustration of the charge order enables the SC to prevail for a much wider range of strong e -ph interaction.

B. Coexistence phase

In order to gain more insight into the SC/CDW coexistence phase, we turn on a tiny pinning potential consistent with the periodicity of the CDW. We then compute the expectation value of local electron density $n_i = \langle c_i^\dagger c_i \rangle$ and its mean-square fluctuation $\Delta n_i^2 = \langle \hat{n}_i^2 \rangle - \langle \hat{n}_i \rangle^2$. The result for the electron

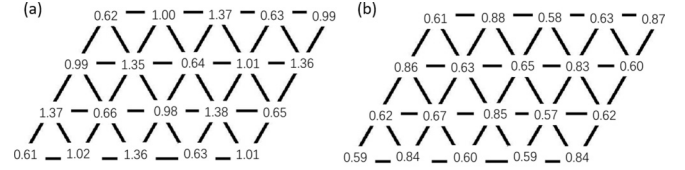


FIG. 3. The local density (a) and its mean-square fluctuations (b) in the CDW-SC coexistent phase on the triangular lattice at $\hbar\omega/E_F = 0.1$. The calculation is carried out at zero temperature for $L = 12$ and $\lambda = 0.5$.

density distribution is shown in Fig. 3(a), which clearly reveals the $\sqrt{3} \times \sqrt{3}$ periodicity. The results for Δn^2 are presented in Fig. 3(b). It shows a significantly stronger charge fluctuation on the lattice sites with $\langle n_i \rangle \approx 1$. In addition, we have also computed the SC correlation function in the coexistence phase. Remarkably, the correlation is significantly stronger among the sites with larger charge fluctuation. These results suggest the SC coherence within the CDW is enabled by the “flippable” sites, which in turn is caused by the geometric frustration.

IV. HALF-FILLING AND NONZERO TEMPERATURES

A. SC and CDW susceptibilities

Next, we fix the temperature and linear lattice size to $k_B T = t/16$ and $L = 12$, where k_B is Boltzmann weight, and compute the SC and CDW susceptibilities as a function of $\lambda \in [0.0, 0.5]$. For the triangular lattice, the CDW susceptibility peaks at wave vector $\mathbf{Q} = (\pm 4\pi/3, 0)$ as shown in Fig. 1(b). Moreover as shown in Fig. 4(a), the SC susceptibility is enhanced with increasing λ until $\lambda \approx 0.4$. For larger λ the CDW susceptibility rises which suppresses the SC susceptibility. For comparison, we also plot the CDW and SC susceptibility for the square lattice in Fig. 4(b). Similar to the triangular lattice result, when CDW ordering tendency gets stronger, SC is suppressed. Moreover, upon taking the absolute scale of the susceptibility into account, it is seen that the CDW/SC susceptibility is strongly suppressed/enhanced on the triangular lattice.

B. Kosterlitz-Thouless transition

We estimate the SC Kosterlitz-Thouless (KT) transition temperature T_c through the well-known scaling behavior of the SC susceptibility (χ_{SC}) at the KT transition: $\chi_{SC} \sim L^{2-\eta}$, where $\eta = 0.25$. Upon fixing $\lambda = 0.4$ for the triangular lattice and $\lambda = 0.2$ for the square lattice (these are the λ values at which the SC susceptibility is the strongest at $T = t/16$), we plot $L^{-2+\eta}\chi_{SC}$ as a function of temperature in Fig. 4. The crossing of the curves for different L marks the phase transition. The result suggests that the transition temperature for triangular lattice is $T_c \approx t/10$ [Fig. 4(a)]. In contrast, for the square lattice no crossing is observed for $T \geq t/16$ [Fig. 4(b)]. When combined with the zero-temperature result, this suggests the absence of SC. This comparison again provides the evidence for frustration-enhanced SC on triangular lattice.

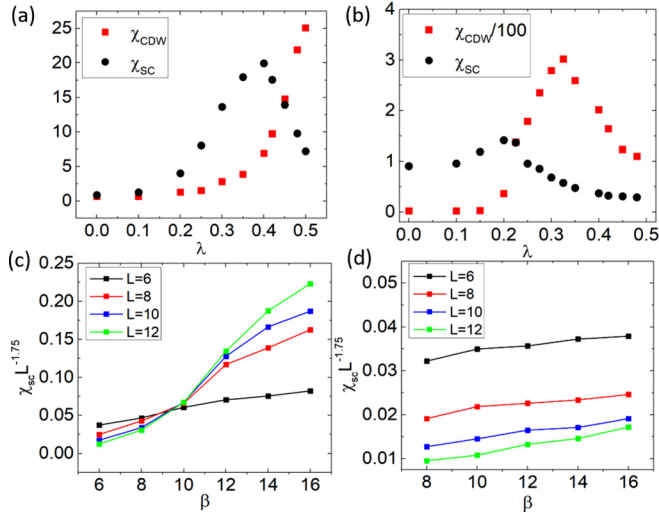


FIG. 4. (a) The SC and CDW susceptibilities on the triangular lattice for $\hbar\omega/E_F = 0.3$. The wave vectors of the SC and CDW are $(0, 0)$ and $(4\pi/3, 0)$, respectively. (b) The SC and CDW susceptibilities for $\hbar\omega/E_F = 0.3$ on a square lattice. The wave vectors of the SC/CDW are $(0, 0)$ and (π, π) , respectively. The results in (a) and (b) are obtained at $T = t/16$ and $L = 12$. (c) The scaled SC susceptibility, $\chi_{SC} L^{-2-\eta_c}$ where $\eta_c = 0.25$, for the triangular lattice. The e-ph coupling is set to $\lambda = 0.4$. Here, β is inverse temperature in unit of $1/t$. The crossing point indicates the Kosterlitz-Thouless transition temperature: $T_c \approx t/10$. (d) The same plot for the square lattice, here λ is set to 0.2. The absence of the crossing implies that, if it exists, the SC transition temperature is below the lowest temperature we calculated. The results in (c) and (d) are obtained for $L = 12$ and $\hbar\omega/E_F = 0.3$. The error bars are smaller than the data points in the figure.

C. Pseudogap

Stimulated by the phenomenology of the cuprates, single-particle gaps above the SC transition are of considerable interests. In the Holstein model, we expect a single-particle gap to accompany the bipolaron formation. Moreover, because the hopping of bipolarons is suppressed at large e-ph coupling, which results in a small SC phase stiffness, we expect a pseudogap can persist above the SC transition temperature T_c .

We have computed the single-particle gap for both triangular and square lattices at half-filling through analytical continuation [57,58]. As shown in Figs. 5(a) and 5(b), the pseudogap at $T = t/8$ (which is above the highest T_c for both systems) undergoes a sharp upturn around the λ value where the CDW susceptibility rises (which signifies the bipolaron formation). In Appendix F we study the pseudogap onset temperature for the half-filled triangular lattice. The result $T^* \approx 0.45t$ is considerably above the Kosterlitz-Thouless transition temperature.

V. AWAY FROM HALF-FILLING, AND THE EFFECT OF DECREASING $\hbar\omega/E_F$

Doping away from half-filling further suppresses the CDW ordering. In Appendix B we report the result for 15% electron-doped triangular and square lattices.

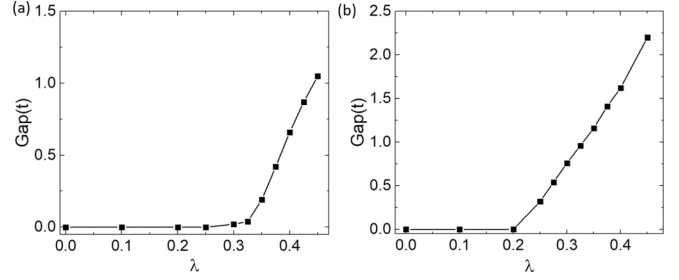


FIG. 5. (a) The evolution of single-particle gap, extracted from the spectral function $A(\mathbf{k}_F, \omega)$, at the Fermi momentum as a function of λ on a triangular lattice. (b) The same plot for the square lattice. The results are obtained for $\hbar\omega/E_F = 0.3$, $L = 12$, and $T = t/8$.

Compared with the results at half-filling, SC/CDW are obviously enhanced/suppressed.

Decreasing the phonon frequency makes the Holstein oscillator more classical. Due to the diminished quantum fluctuations, bipolarons are easier to form and localize. As a result, CDW correlation gets stronger and SC becomes weaker.

VI. CONCLUSION

We have studied the effects of frustrating charge order on superconductivity using the Holstein model through sign-problem-free QMC simulation. We conclude that frustrating the charge order is a powerful way to enhance superconductivity. In particular, it enables a novel coexistence phase where superconducting coherence develops in the charge-ordered phase. When the electron-phonon coupling is sufficiently strong, the real-space Cooper pairing occurs, namely, bipolarons form. On the unfrustrated lattice, as suggested by previous works [14,52], the bipolarons form a CDW ordered state. In such state, the bipolarons become localized, hence destroy superconducting coherence. Our work reveals that when CDW order is frustrated by the lattice geometric frustration, the bipolarons remain mobile due to the flappable sites. As a result, superconducting coherence can be established, hence allowing superconductivity to benefit from a larger range of electron-phonon coupling strength. We believe that our study will shed new light on the future search for the high-temperature superconductivity in the materials with strong electron-phonon coupling.

ACKNOWLEDGMENTS

This work was primarily funded by the U. S. Department of Energy, Office of Science, Office of Basic Energy Sciences, Materials Sciences and Engineering Division under Contract No. DE-AC02-05-CH11231 (Theory of Materials program KC2301). Z.-X.L. and D.-H.L. also acknowledge support from the Gordon and Betty Moore Foundation's EPIC initiative, Grant No. GBMF4545. M.L.C. also acknowledges support from the National Science Foundation Grant No. DMR-1508412. The computational part of this research is supported by the U. S. Department of Energy, Office of Science, Office of Advanced Scientific Computing Research, Scientific Discovery through Advanced Computing (SciDAC) program.

Computational resources are provided by the National Energy Research Scientific Computing Center (NERSC).

APPENDIX A: DETAILS OF THE QUANTUM MONTE CARLO SIMULATION

We apply both the finite-temperature and projector determinant QMC algorithm to study Eq. (1) in main text. In the finite-temperature simulation, the grand canonical ensemble averages of observables are evaluated through $\langle \hat{O} \rangle = \text{Tr}[\hat{O}e^{-\beta\hat{H}}]/\text{Tr}[e^{-\beta\hat{H}}]$. Here, β is the inverse temperature. The values studied in this paper are $4/t \leq \beta \leq 16/t$, where t is electron's nearest-neighbor hopping matrix element. The imaginary time is discretized with the time step $\Delta\tau = 0.1/t$. We have checked that the results do not change upon further decrease of $\Delta\tau$.

In the projector QMC, we evaluate the ground-state expectation values of observables according to $\langle \hat{O} \rangle = \langle \psi_0 | \hat{O} | \psi_0 \rangle / \langle \psi_0 | \psi_0 \rangle = \lim_{\theta \rightarrow \infty} \{ \langle \psi_T | e^{-\theta H} \hat{O} e^{-\theta H} | \psi_T \rangle / \langle \psi_T | e^{-2\theta H} | \psi_T \rangle \}$, where $|\psi_T\rangle$ is a trial state. In our simulation, the trial state is chosen as the ground state of the noninteracting Hamiltonian. In this work, θ is set to $30/t$, and we have checked the convergence of the results against further increase of θ . Like the finite-temperature calculations we have checked that the imaginary-time step $\Delta\tau = 0.1/t$ is sufficient to guarantee the convergence of the result.

Finally, in both the zero- and finite-temperature calculations we carry out both single-site and block updates to ensure the statistical independence in our Monte Carlo sampling [53]. Because the phonon field is strongly correlated in imaginary-time direction, especially for small $\Delta\tau$, we implement block update to reduce the autocorrelation time of the Monte Carlo sampling in our simulation. In the scheme of block update, we simultaneously update the phonon fields at a given site for all the imaginary time. Unfortunately, the implement of block update severely slows down the simulation in DQMC. In our computation, we perform one to five block updates between each space-time local update sweep, depending on the temperature in the simulation. At the zero-temperature computation or finite-temperature computation for $T \leq t/12$, we perform five block updates between each space-time local update sweep. In our simulation, we run 240 independent Markov chains with 600–5000 space-time sweeps, depending on the temperature and system sizes, after the procedure of thermalization for each data point. In some computations for low temperature and zero temperature, we run 480 independent Markov chains.

APPENDIX B: NONZERO TEMPERATURE SC AND CDW SUSCEPTIBILITIES FOR DOPED TRIANGULAR AND SQUARE LATTICES

Intuitively, incommensurate filling factors resulting from doping should suppress the CDW order and enhance the SC pairing. To check this intuition, we calculate the SC and CDW susceptibilities for different values of λ at temperature $T = t/16$ for lattices with linear dimension $L = 12$. The doping is chosen to be 15%, i.e., $\langle \hat{n} \rangle = 1.15$. The results are shown in Fig. 6. Compared with half-filling, the CDW susceptibility is suppressed by doping, while the SC susceptibility is

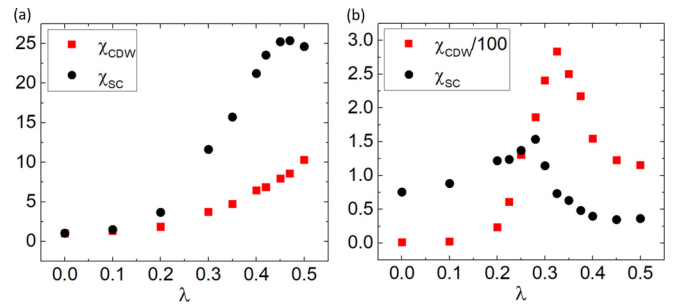


FIG. 6. (a) The SC and CDW susceptibilities for a doped ($\langle n \rangle = 1.15$) triangular lattice. (b) The SC and CDW susceptibilities for a doped ($\langle n \rangle = 1.15$) square lattice. The results are obtained under the parameter choice $\hbar\omega/E_F = 0.3$, $L = 12$, and $T = t/16$. The error bars are smaller than the data points.

enhanced. Moreover by comparing Figs. 6(a) and 6(b) we conclude that for a doped system, lattice frustration remains very effective in suppressing/enhancing CDW/SC orders.

APPENDIX C: NONZERO TEMPERATURE SC AND CDW SUSCEPTIBILITIES FOR A TRIANGULAR LATTICE AT $\hbar\omega/E_F = 0.1$

Here, the temperature is set to $T = t/16$ and linear system size is $L = 12$. In Fig. 7 we show the SC and CDW susceptibilities as a function of λ . Qualitatively, the behaviors of the SC and CDW susceptibilities are similar to those for $\hbar\omega/E_F = 0.3$. However, it is notable that lower $\hbar\omega/E_F$ enhances the CDW while suppressing the SC ordering tendencies.

APPENDIX D: FINITE-SIZE SCALING ANALYSIS OF THE ZERO-TEMPERATURE SC AND CDW ORDERS FOR TRIANGULAR AND SQUARE LATTICES

We perform projector QMC simulation to study the ground-state properties of the Holstein model on the triangular lattice. The Fourier transforms of the SC and CDW correlation functions at momentum $(0, 0)$ (SC) and $(4\pi/3, 0)$ (CDW) are shown in Fig. 8. When extrapolated to $L = \infty$ the finite values

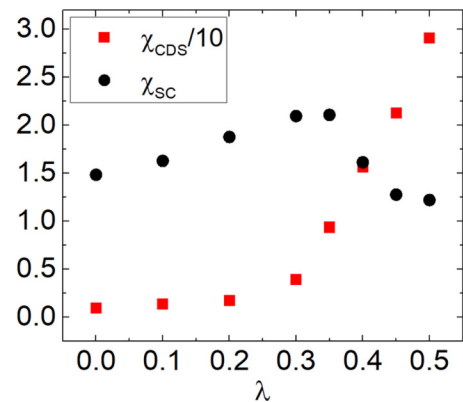


FIG. 7. The SC and CDW susceptibility on a triangular lattice for $\hbar\omega/E_F = 0.1$. The temperature is $T = t/16$ and the linear system size $L = 12$. The error bars are smaller than the data points in the figure.

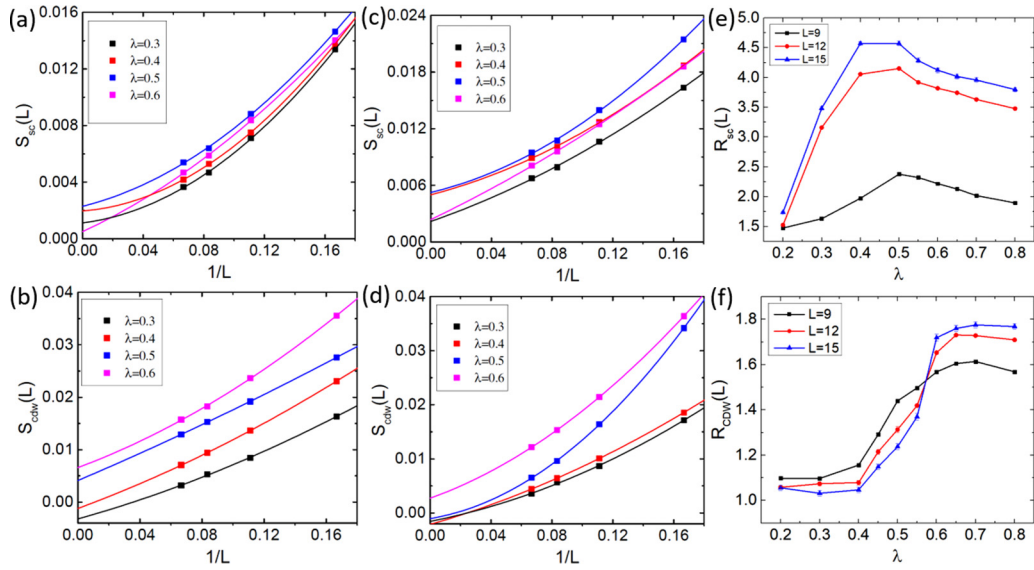


FIG. 8. (a) Finite-size scaling analysis of the peak of the Fourier-transformed SC correlation function on a triangular lattice for $L = 6, 9, 12, 15$ and $\hbar\omega/E_F = 0.1$. (b) Finite-size scaling analysis for the peak of the CDW structure factors on a triangular lattice for $L = 6, 9, 12, 15$ and $\hbar\omega/E_F = 0.1$. (c) The same as (a) for $\hbar\omega/E_F = 0.3$. (d) The same as (b) for $\hbar\omega/E_F = 0.3$. (e) The RG-invariant ratio $R_{SC}(L)$ on triangular lattice for $\hbar\omega/E_F = 0.3$. (f) The $R_{SC}(L)$ on triangular lattice for $\hbar\omega/E_F = 0.3$. In this figure, the temperature is $t/16$ and linear system size $L = 12$.

of these quantities indicates long-range order. In Figs. 8(a) to 8(d) the data are fit by second-order polynomials in $1/L$. At $\hbar\omega/E_F = 0.1$, the SC order [Fig. 8(a)] is persistent in the entire range of λ ($0.2 \leq \lambda \leq 0.8$). However, the CDW structure factors [Fig. 8(b)] are extrapolated to zero or negative values within error bars when $\lambda < 0.4$, while extrapolated to finite values when $\lambda > 0.4$. The result suggests that the ground state is a coexistent phase of SC and $\sqrt{3} \times \sqrt{3}$ CDW when e-ph coupling is stronger than 0.4. For $\hbar\omega/E_F = 0.3$, the SC correlations [Fig. 8(c)] also extrapolate to a finite value in the entire range of λ we studied. The CDW correlations [Fig. 8(d)], on the other hand, are extrapolated to finite values only when $\lambda > 0.6$. To verify this result, we also calculated the RG-invariant ratio $R = S(Q)/S(Q + \delta q)$ as a function of lattice size, where Q is peak momentum of Fourier-transformed correlation function, and δq is the minimum allowed momentum quantum on lattice. $R(L)$ has smaller finite-size scaling corrections than correlation functions, hence is a powerful tool for investigating the thermal or quantum phase and phase transition on finite lattices. In the long-range-ordered phase, $R(L)$ should diverge for $L \rightarrow \infty$, while $R(L) \rightarrow 0$ for $L \rightarrow \infty$ in disordered phase. At the critical point, $R(L)$ collapses to a finite value for different L due to scaling invariance. We present the results of RG-invariant ratio for $\hbar\omega/E_F = 0.1$ in Figs. 2(c) and 2(d) and $\hbar\omega/E_F = 0.3$ in Fig. 8. The results are qualitatively consistent with the conclusion drawn from the extrapolation of the correlation functions. For $\hbar\omega/E_F = 0.1$, we observe a quantum phase transition from the SC phase to a SC and CDW coexistent phase around $\lambda \approx 0.42$. For $\hbar\omega/E_F = 0.3$, the CDW order coexists with SC when $0.6 \lesssim \lambda \leq 0.8$.

For comparison, we have also studied the Holstein model on square lattice. In this study we turn on a next-nearest-neighbor hopping $t_2 = -0.2t_1$ to get rid of Fermi-surface

nesting. We perform finite-size scaling analysis of the SC and CDW correlation functions for $\hbar\omega/E_F = 0.1$ and 0.3 , for $0.2 \leq \lambda \leq 0.8$. The results of RG-invariant ratio, as plotted in Fig. 9, clearly show that the ground state possesses CDW long-range order and no SC order for both $\hbar\omega/E_F = 0.1$ and 0.3 . This result, combined with those for the triangular lattice, suggests that CDW order is strongly suppressed by geometric frustration, which enables SC pairing to exist in a larger range of e-ph coupling strength.

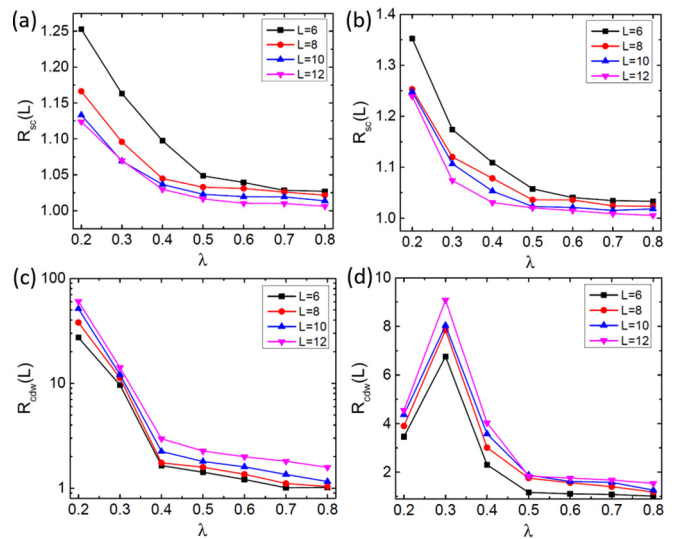


FIG. 9. The RG-invariant ratios $R_{SC}(L)$ and $R_{CDW}(L)$ for the square lattice. (a) The $R_{SC}(L)$ at $\hbar\omega/E_F = 0.1$, and (b) the $R_{SC}(L)$ at $\hbar\omega/E_F = 0.3$. (c) The $R_{CDW}(L)$ at $\hbar\omega/E_F = 0.1$, and (d) the $R_{CDW}(L)$ at $\hbar\omega/E_F = 0.3$.

APPENDIX E: LOCAL DENSITY AND DENSITY FLUCTUATION DISTRIBUTION IN SC AND CDW COEXISTENT PHASE

We compute the average of the charge density and its mean-square fluctuation in the SC and CDW coexistent phase. We employ projector QMC for $\lambda = 0.5$ and $\hbar\omega/E_F = 0.1$. A tiny modulated chemical potential consistent with CDW periodicity is added to pin the CDW to one of three degenerate CDW patterns. In particular, we applied a modulated chemical potential with amplitude $\delta = 0.02$ and have checked that such pinning potential do not affect the intrinsic values of the SC and CDW correlation functions. The result of averaged charge density is shown in Fig. 4(a), which clearly reveals the $\sqrt{3} \times \sqrt{3}$ CDW pattern in Fig. 1(a). The charge density on the three sublattices is $(1 + a, 1 - a)$. More importantly, as shown in Fig. 4(b), the charge fluctuations are significantly stronger on the sublattice where the averaged density is approximately unity. Since SC order requires charge fluctuation, we expect that SC correlation to be bigger on such sublattice. This is verified by our unbiased QMC simulation.

APPENDIX F: ELECTRON SPECTRAL FUNCTION ON TRIANGULAR AND SQUARE LATTICE

In order to investigate the existence of pseudogap in the Holstein model, we compute the electron spectral function through analytical continuation of the imaginary-time Green's function. The approach of analytical continuation that we use in our computation is stochastic maximum entropy method [57,58]. We obtain the electron spectral functions at different points on the Fermi surface. Here, we present the spectral function $A(k_F, \omega)$ at momentum point where the pseudogap is the minimum. The results of $A(k_F, \omega)$ for $\lambda = 0.4$ on triangular at temperatures $T = t/18, t/12, t/8$ are shown in Fig. 10 where $t/8$ is above the T_c for triangular lattice (the square lattice does not show a SC transition). We estimate the value of single-particle gap from the peaks of spectral function $A(k_F, \omega)$. In Fig. 5, we present the values of spectral gap for several values of λ on triangular and square lattices. The pseudogap above T_c undergoes a sharp upturn around λ value where CDW susceptibility rises. We also present the single-particle gap as a function of temperature for $\lambda = 0.4$ on triangular in Fig. 10(d). From this result, we estimate the onset temperature of pseudogap $T^* \approx 0.45t$.

APPENDIX G: SCALING BEHAVIOR OF THE SC SUSCEPTIBILITY FOR $T \gtrsim T_c$ AND THE FINITE-SIZE SCALING ANALYSIS FOR THE SC SUSCEPTIBILITY BELOW T_c

In this Appendix, we present the scaling behavior of the SC susceptibility for $T \gtrsim T_c$. In addition, we also present the finite-size scaling analysis of the SC susceptibility for $T < T_c$. Both results are obtained on triangular lattice.

In a 2D superconductor, the quasi-long-range SC order implies that the SC susceptibility should diverge with the system size in a power-law fashion below the Kosterlitz-Thouless (KT) transition temperature T_c . In addition, for $T \gtrsim T_c$ the KT phase transition predicts the following scaling behavior for the

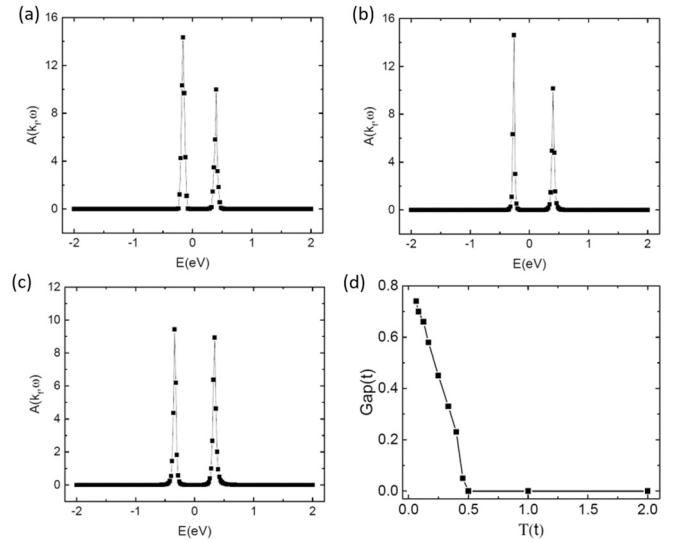


FIG. 10. The electron spectral function $A(k_F, \omega)$ for $\lambda = 0.4$ on triangular lattice at various temperatures: (a) $T = t/8$; (b) $T = t/12$; (c) $T = t/16$. The results clearly show that spectral gap survives above the SC transition temperature $t/10$. (d) The single-particle gap on triangular lattice for $\lambda = 0.4$ as a function of temperature. The pseudogap onset temperature is estimated to be $T^* \approx 0.45t$.

superconducting susceptibility:

$$\chi_{SC}(L, T) = L^{2-\eta} f(L/\xi), \quad (G1)$$

where $\eta = \frac{1}{4}$ and ξ is correlation length with the following temperature dependence:

$$\xi = \exp[A/\sqrt{T - T_c}]. \quad (G2)$$

Here, $f(L/\xi)$ is a scaling function whose numerical value depends on the microscopic details. In Fig. 11(a) we collapse the data for different temperatures and system sizes according to Eqs. (G1) and (G2). The temperature range in this analysis is $k_B T \in [t/6, t/10]$ and the system sizes are $L = 6, 8, 10, 12$. The best data collapse is achieved by choosing $A = 0.32$ and $k_B T_c = t/10$. The excellent quality of the data collapsing is a confirmation that the SC transition is indeed in the KT universality class.

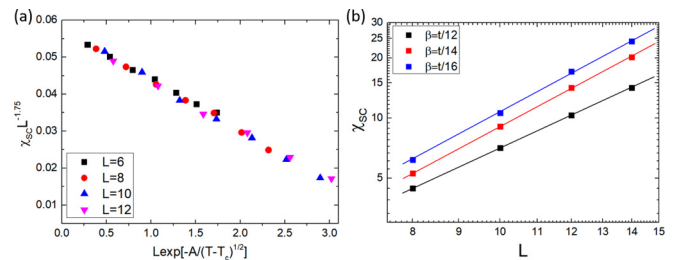


FIG. 11. (a) Data collapse analysis of the SC susceptibility in the regime close to transition temperature T_c . By choosing $T_c = t/10$ and $A = 0.32$, it is clearly shown that the SC susceptibility for different T and L can be fitted by a single scaling function consistent with KT transition. (b) The log-log plot of the SC susceptibility as a function of linear system size L below transition temperature T_c . The error bars are smaller than the data points in the figure.

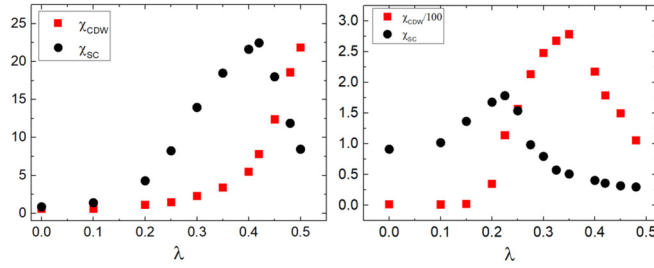


FIG. 12. (a) The SC and CDW susceptibilities on the triangular lattice for $\hbar\omega/E_F = 0.3$ and $\Delta\omega = 0.2\omega$. The wave vectors of the SC and CDW are $(0, 0)$ and $(4\pi/3, 0)$, respectively. (b) The SC and CDW susceptibilities on the triangular lattice for $\hbar\omega/E_F = 0.3$ and $\Delta\omega = 0.2\omega$. The wave vectors of the SC and CDW are $(0, 0)$ and (π, π) , respectively. The error bars are smaller than the data points in the figure.

In Fig. 11(b) we present the SC susceptibility below T_c as a function of system size L . The result is consistent with a power-law divergence with the power decreases as a function of increasing temperature. This is consistent with the known behavior of the SC order-parameter correlation function below T_c .

APPENDIX H: EFFECT OF PHONON BAND DISPERSION

In the Holstein model the phonon is dispersionless. In this Appendix, we investigate the effect of a nonzero phonon

dispersion on the SC and CDW susceptibilities. We modify the phonon Hamiltonian by adding a nearest-neighbor coupling term between the displacement field:

$$H_p = \sum_i \left(\frac{\hat{P}_i^2}{2M} + \frac{K}{2} \hat{X}_i^2 \right) + \frac{K_2}{2} \sum_{\langle ij \rangle} (\hat{X}_i - \hat{X}_j)^2. \quad (\text{H1})$$

The resulting bare phonon dispersion is given by $E_p(\vec{k}) = \sqrt{\frac{K}{M} + \frac{2K_2}{M} [2 - \cos(\vec{a}_1 \cdot \vec{k}) - \cos(\vec{a}_2 \cdot \vec{k})]}$ on square lattice, where $\vec{a}_1 = (1, 0)$ and $\vec{a}_2 = (0, 1)$, and $E_p(\vec{k}) = \sqrt{\frac{K}{M} + \frac{2K_2}{M} [3 - \cos(\vec{a}_1 \cdot \vec{k}) - \cos(\vec{a}_2 \cdot \vec{k}) - \cos(\vec{a}_3 \cdot \vec{k})]}$ on triangular lattice, where $\vec{a}_1 = (1, 0)$, $\vec{a}_2 = (\frac{1}{2}, \frac{\sqrt{3}}{2})$, $\vec{a}_3 = (-\frac{1}{2}, \frac{\sqrt{3}}{2})$. The associated bare phonon bandwidth is given by $\Delta\omega = E_p(\vec{k}_{\max}) - E_p(\vec{k}_{\min})$, where $E_p(\vec{k}_{\max})/E_p(\vec{k}_{\min})$ is the energy at the band top and bottom. In the following, we choose a $\Delta\omega = 0.2\omega$, where $\hbar\omega = 0.3E_F$ is the average phonon frequency. We set the inverse temperature to $\beta = 16/t$ and compute the SC and CDW susceptibility as a function of λ for both the square and triangular lattice, the results of which are shown in Fig. 12. When comparing them to the corresponding results in the dispersion-free limit, we see a qualitative agreement. Specifically, for large λ the CDW susceptibility rises which tends to suppress the SC susceptibility. Moreover, looking at the absolute scale of susceptibility, we find that the CDW/SC susceptibility is strongly suppressed/enhanced on the triangular lattice. Upon a quantitative comparison, we find the the CDW susceptibility is slightly suppressed and the SC susceptibility is slightly enhanced by the nonzero phonon dispersion.

-
- [1] M. L. Cohen and P. W. Anderson, in *Superconductivity in d- and f-Metals*, edited by H. C. Wolfe and D. H. Douglass, AIP Conf. Proc. No. 4 (AIP, New York, 1972), p. 17.
- [2] C. M. Varma and A. L. Simons, *Phys. Rev. Lett.* **51**, 138 (1983).
- [3] F. C. Zhang, Masao Ogata, and T. M. Rice, *Phys. Rev. Lett.* **67**, 3452 (1991).
- [4] J. K. Freericks, M. Jarrell, and D. J. Scalapino, *Phys. Rev. B* **48**, 6302 (1993).
- [5] R. T. Scalettar, N. E. Bickers, and D. J. Scalapino, *Phys. Rev. B* **40**, 197 (1989).
- [6] F. Marsiglio, *Phys. Rev. B* **42**, 2416 (1990).
- [7] E. Jeckelmann and S. R. White, *Phys. Rev. B* **57**, 6376 (1998).
- [8] G. Wellein and H. Fehske, *Phys. Rev. B* **56**, 4513 (1997).
- [9] D. Meyer, A. C. Hewson, and R. Bulla, *Phys. Rev. Lett.* **89**, 196401 (2002).
- [10] A. S. Alexandrov, *Europhys. Lett.* **56**, 92 (2001).
- [11] J. Bauer, J. E. Han, and O. Gunnarsson, *Phys. Rev. B* **84**, 184531 (2011).
- [12] E. W. Carlson, V. J. Emery, S. A. Kivelson, and D. Orgad, *Concepts in High Temperature Superconductivity, in Superconductivity: Conventional and Unconventional Superconductors*, edited by K. H. Bennemann and J. B. Ketterson (Springer, Berlin, 2008), pp. 1225–1348.
- [13] H. Fehske and S. A. Trugman, Numerical solution of the Holstein polaron problem, in *Polarons in Advanced Materials*, edited by A. S. Alexandrov, Springer Series in Material Sciences (Springer, Dordrecht, 2007), Vol. 103, pp. 393–461.
- [14] I. Esterlis, B. Nosarzewski, E. W. Huang, B. Moritz, T. P. Devereaux, D. J. Scalapino, and S. A. Kivelson, *Phys. Rev. B* **97**, 140501(R) (2018).
- [15] H. Seo, K. Tsutsui, M. Ogata, and J. Merino, *J. Phys. Soc. Jpn.* **75**, 114707 (2006).
- [16] I. Leonov, A. N. Yaresko, V. N. Antonov, M. A. Korotin, and V. I. Anisimov, *Phys. Rev. Lett.* **93**, 146404 (2004).
- [17] J. Merino, H. Seo, and M. Ogata, *Phys. Rev. B* **71**, 125111 (2005).
- [18] N. Ikeda, H. Ohsumi, K. Ohwada, K. Ishii, T. Inami, K. Kakurai, Y. Murakami, K. Yoshii, S. Mori, Y. Horibe, and H. Kito, *Nature (London)* **436**, 1136 (2005).
- [19] O. I. Motrunich and P. A. Lee, *Phys. Rev. B* **69**, 214516 (2004).
- [20] K. Matsuno, T. Katsufuji, S. Mori, Y. Moritomo, A. Machida, E. Nishibori, M. Takata, M. Sakata, N. Yamamoto, and H. Takagi, *J. Phys. Soc. Jpn.* **70**, 1456 (2001).
- [21] P. Fulde, *J. Phys.: Condens. Matter* **16**, S591 (2004).
- [22] H. Mori, S. Tanaka, and T. Mori, *Phys. Rev. B* **57**, 12023 (1998).
- [23] G. H. Wannier, *Phys. Rev.* **79**, 357 (1950); *Phys. Rev. B* **7**, 5017(E) (1973).
- [24] K. Husimi and Itiro Syôzi, *Prog. Theor. Phys.* **5**, 177 (1950).
- [25] R. M. F. Houtappel, *Physica (Amsterdam)* **16**, 425 (1950).
- [26] J. Stephenson, *J. Math. Phys.* **11**, 413 (1970).
- [27] O. Nagai, S. Miyashita, and T. Horiguchi, *Phys. Rev. B* **47**, 202 (1993).
- [28] R. Moessner, S. L. Sondhi, and P. Chandra, *Phys. Rev. Lett.* **84**, 4457 (2000).

- [29] R. Moessner and S. L. Sondhi, *Phys. Rev. B* **63**, 224401 (2001).
- [30] R. G. Melko, A. Paramekanti, A. A. Burkov, A. Vishwanath, D. N. Sheng, and L. Balents, *Phys. Rev. Lett.* **95**, 127207 (2005).
- [31] D. Heidarian and K. Damle, *Phys. Rev. Lett.* **95**, 127206 (2005).
- [32] S. Wessel and M. Troyer, *Phys. Rev. Lett.* **95**, 127205 (2005).
- [33] M. Boninsegni and N. Prokof'ev, *Phys. Rev. Lett.* **95**, 237204 (2005).
- [34] S. R. Hassan, L. de Medici, and A.-M. S. Tremblay, *Phys. Rev. B* **76**, 144420 (2007).
- [35] F. F. Assaad and H. G. Evertz, *Computational Many-Particle Physics*, Lecture Notes in Physics (Springer, Berlin, 2008), Vol. 739, pp. 277–356.
- [36] C. Wu and S.-C. Zhang, *Phys. Rev. B* **71**, 155115 (2005).
- [37] Z.-X. Li, Y.-F. Jiang, and H. Yao, *Phys. Rev. B* **91**, 241117(R) (2015).
- [38] Z.-X. Li, Y.-F. Jiang, and H. Yao, *Phys. Rev. Lett.* **117**, 267002 (2016).
- [39] Z.-C. Wei, C. Wu, Y. Li, S. Zhang, and T. Xiang, *Phys. Rev. Lett.* **116**, 250601 (2016).
- [40] L. Wang, Y.-H. Liu, M. Iazzi, M. Troyer, and G. Harcos, *Phys. Rev. Lett.* **115**, 250601 (2015).
- [41] Z.-X. Li and H. Yao, *Annu. Rev. Condens. Matter Phys.* **10**, 337 (2019).
- [42] R. M. Noack, D. J. Scalapino, and R. T. Scalettar, *Phys. Rev. Lett.* **66**, 778 (1991).
- [43] F. F. Assaad and T. C. Lang, *Phys. Rev. B* **76**, 035116 (2007).
- [44] M. Hohenadler, H. G. Evertz, and W. von der Linden, *Phys. Rev. B* **69**, 024301 (2004).
- [45] E. A. Nowadnick, S. Johnston, B. Moritz, R. T. Scalettar, and T. P. Devereaux, *Phys. Rev. Lett.* **109**, 246404 (2012).
- [46] S. Li, E. A. Nowadnick, and S. Johnston, *Phys. Rev. B* **92**, 064301 (2015).
- [47] N. C. Costa, T. Blommel, W.-T. Chiu, G. Batrouni, and R. T. Scalettar, *Phys. Rev. Lett.* **120**, 187003 (2018).
- [48] M. Weber and M. Hohenadler, *Phys. Rev. B* **98**, 085405 (2018).
- [49] C. Chen, X. Y. Xu, Z. Y. Meng, and M. Hohenadler, *Phys. Rev. Lett.* **122**, 077601 (2019).
- [50] Y.-X. Zhang, W.-T. Chiu, N. C. Costa, G. G. Batrouni, and R. T. Scalettar, *Phys. Rev. Lett.* **122**, 077602 (2019).
- [51] C. Chen, X. Y. Xu, J. Liu, G. Batrouni, R. Scalettar, and Z. Y. Meng, *Phys. Rev. B* **98**, 041102(R) (2018).
- [52] I. Esterlis, S. Kivelson, and D. Scalapino, *Phys. Rev. B* **99**, 174516 (2019).
- [53] R. T. Scalettar, R. M. Noack, and R. R. P. Singh, *Phys. Rev. B* **44**, 10502 (1991).
- [54] G. Sugiyama and S. Koogin, *Ann. Phys.* **168**, 1 (1986).
- [55] S. Sorella, S. Baroni, R. Car, and M. Parrinello, *Europhys Lett.* **8**, 663 (1989).
- [56] S. R. White, D. J. Scalapino, R. L. Sugar, E. Y. Loh, J. E. Gubernatis, and R. T. Scalettar, *Phys. Rev. B* **40**, 506 (1989).
- [57] A. W. Sandvik, *Phys. Rev. B* **57**, 10287 (1998).
- [58] K. S. D. Beach, [arXiv:cond-mat/0403055](https://arxiv.org/abs/cond-mat/0403055).